Environmental Modelling and Software 157 (2022) 105528

Contents lists available at ScienceDirect

Environmental Modelling and Software

journal homepage: www.elsevier.com/locate/envsoft

AIRCC-Clim: A user-friendly tool for generating regional probabilistic climate change scenarios and risk measures

Francisco Estrada [a,b,c,*], Oscar Calderón-Bustamante [a], Wouter Botzen [b,d], Julián A. Velasco [a], Richard S.J. Tol [e,f,g,h,i]

[a] Instituto de Ciencias de la Atmósfera y Cambio Climático, Universidad Nacional Autónoma de México, CDMX, Mexico
[b] Institute for Environmental Studies, VU Amsterdam, Amsterdam, the Netherlands
[c] Programa de Investigación en Cambio Climático, Universidad Nacional Autónoma de México, CDMX, Mexico
[d] Utrecht University School of Economics (U.S.E.), Utrecht University, Utrecht, Netherlands
[e] Department of Economics, University of Sussex, Falmer, UK
[f] Department of Spatial Economics, Vrije Universiteit, Amsterdam, the Netherlands
[g] Tinbergen Institute, Amsterdam, the Netherlands
[h] CESifo, Munich, Germany
[i] Payne Institute for Public Policy, Colorado School of Mines, Golden, CO, USA

ARTICLE INFO

Keywords:
Climate change scenarios
Climate model emulator
Impact
Vulnerability and adaptation assessment
Stochastic simulation

ABSTRACT

Complex physical models are the most advanced tools available for producing realistic simulations of the climate system. However, such levels of realism imply high computational cost and restrictions on their use for policymaking and risk assessment. Two central characteristics of climate change are uncertainty and that it is a dynamic problem in which international actions can significantly alter climate projections and information needs, including partial and full compliance of global climate goals. Here we present AIRCC-Clim, a simple climate model emulator that produces regional probabilistic climate change projections of monthly and annual temperature and precipitation, as well as risk measures, based both on standard and user-defined emissions scenarios for six greenhouse gases. AIRCC-Clim emulates 37 atm-ocean coupled general circulation models with low computational and technical requirements for the user. This standalone, user-friendly software is designed for a variety of applications including impact assessments, climate policy evaluation and integrated assessment modelling.

1. Software availability

AIRCC-Clim can be downloaded at no cost from https://sites.google.com/view/aircc-lab-airccclim/aircc-clim.

2. Introduction

Climate change projections are one of the main inputs for assessing the potential consequences of different socioeconomic development pathways and international climate policy on natural and human systems. Due to the complexity of the systems involved and their interactions, climate projections are inherently uncertain (Gay and Estrada 2010; Curry and Webster 2011; Knutti and Sedláček 2012). Moreover, computational and technical costs of state-of-the-art physical models allow exploration of only a small fraction of the range of possible climate futures and hinder assessing risk through probabilistic scenarios (Knutti et al., 2010; Sanderson et al., 2015). For most decision-makers and researchers, these costs make it infeasible to explore how current and hypothetical changes in international mitigation policy can influence future warming and its consequences for society. In a time of proactive international mitigation policy, the dynamic nature of projecting future climate becomes even more evident and decision-making requirements can go beyond fixed illustrative emissions scenarios, such as the RCPs (Estrada and Botzen 2021). For example, Nationally Determined Contributions (NDCs) that represent greenhouse gas emission reductions that countries promise as their contributions to the Paris Agreement are currently a key focus of international climate policy. Moreover, due to the nonlinearity of most climate impacts, even small

* Corresponding author. Instituto de Ciencias de la Atmósfera y Cambio Climático, Universidad Nacional Autónoma de México, CDMX, Mexico.
E-mail address: feporrua@atmosfera.unam.mx (F. Estrada).

https://doi.org/10.1016/j.envsoft.2022.105528
Received 29 October 2021; Received in revised form 7 September 2022; Accepted 12 September 2022
Available online 20 September 2022
1364-8152/

deviations from a high-warming trajectory can produce large changes in the associated impacts (Estrada and Botzen 2021; Ignjacevic et al., 2021).

International efforts such as the Coupled Model Intercomparison Project (CMIP), which build and host large databases of climate models' simulations publicly available, have significantly contributed to improving the accessibility and utilization of climate scenarios for the wider research community and decision-makers (Knutti and Sedláček, 2012; Stocker et al., 2013; Taylor et al., 2012). However, many users still face the problem of processing large datasets for adapting them to their particular needs (e.g., temporal frequency and spatial domains). As such, studies and decisions are commonly based on a few illustrative greenhouse gases emissions trajectories and a handful of climate models' simulations which are often selected due to their availability and ease of use, such as WorldClim (Fick and Hijmans 2017). Such a selection of climate model runs can hardly provide a good representation of uncertainty and indicate if a model's projections for a given region may represent extreme realizations in comparison to the majority of other models (Weigel et al., 2010; Sanderson et al., 2015). Even in cases when climate models' performance is assessed, the resulting selection of models does not guaranty that those projections of future climate are reliable (Altamirano del Carmen et al., 2021). Climate model selection remains an unresolved problem as commonly used metrics can be non-informative about the models' ability to reproduce the observed climate change signal and indicate much less about their ability for projecting future climate (Knutti et al., 2010).

Uncertainty is a key characteristic of climate change and how it is understood and included in climate impact assessments can have profound effects on the estimates of the consequences of this phenomenon and on the design of policies to address these consequences (IPCC-TG-ICA 2007; Gay and Estrada 2010). The development of tools and methods for better uncertainty management and for improving the usefulness of the large (thousands of terabytes) databases that are currently available are increasingly relevant research topics. More efficient, simple, and flexible approaches for taking advantage of the available databases can transform data into useful information and knowledge for better assessments of impacts, risks, and climate policy options. Reduced complexity models and emulators of more advanced models allow exploring –at low computational and technical costs for the user– a wide range of possible futures and emissions trajectories, parameterizations, as well as probabilistic assessment of risks for natural and human systems (Meinshausen et al., 2011a; Blanc 2017; Estrada et al., 2020). Integrated assessment modelling benefits from such models and emulators to provide tools for supporting decision-making and providing estimates for cases in which complex climate/impacts model runs are not available.

A notable example of the usefulness of such models is the MAGICC software which has made significant contributions to climate change research, particularly in impact, vulnerability and adaptation (IVA) assessments, and integrated assessment modelling (Wigley 1995; Meinshausen et al., 2011c, a). The MAGICC software has been regularly used in the IPCC reports when simulations produced by general circulation climate models are not available and also in the national climate change assessments of several countries (Conde et al., 2011; IPCC, 2018; 2021). MAGICC6 is able to produce probabilistic global temperature change projections and to capture uncertainties in radiative forcing, as well as in the climate and carbon-cycle responses (Nicholls et al., 2021). The MAGICC7 version is now on-line available (https://magicc.org/).

Here we present AIRCC-Clim (Assessment of Impacts and Risks of Climate Change – Probabilistic Climate Model Emulator), a simple and flexible climate model emulator for producing probabilistic regional projections of monthly and annual temperature and precipitation, as well as risk measures. AIRCC-Clim has five main innovations compared to other reduced complexity models. First, it emulates the results from 37 atm-ocean coupled general circulation models from CMIP phase 5 (CMIP5) included in the Fifth Assessment Report of the IPCC (Stocker et al., 2013) with low computational and technical requirements on the user. Second, it produces spatially explicit ($2.5^\circ \times 2.5^\circ$) climate projections which allows to explore climate change developments at the regional level which can be visualized on maps. Third, it generates global and spatially explicit probabilistic projections of climate change which allows to represent uncertainty about future climate conditions at different spatial scales. Fourth, the model allows constructing a variety of risk measures tailored to the needs of the user, such as the time for exceeding predefined thresholds of changes in climate variables and probabilities of exceedance. Fifth, AIRCC-Clim includes a graphical emissions editor to facilitate introducing new emissions trajectories defined by the user. Additionally, this editor can read external emissions scenarios from Excel files, and it also allows the user to directly modify the emissions scenarios in a table included within the interface. Another advantage that enables easy integration with other software applications is the capability of exporting results in netCDF and GeoTIFF formats, in addition to high quality PNG files. It is a standalone software for Windows and Linux operating systems that requires no programming or advanced technical skills from the user and runs on computers with standard memory and processing resources. AIRCC-Clim is designed for a variety of applications including IVA assessments, integrated assessment modelling, and the quick evaluation of the consequences on global and regional climate of user-defined experiments of international mitigation.

The remainder of this paper is structured as follows: Section 2 describes the AIRCC-Clim model structure and describes in detail each of its modules in terms of data sources, modelling approaches and methods, and their output. This section also describes the file options for exporting climate projections and their characteristics. An application of the model is shown in Section 3 in which the benefits of stringent international mitigation efforts are illustrated in terms of avoided warming, changes in precipitation and risk reduction. Section 4 concludes and discusses model extensions and integration with IVA models.

3. Model structure, data and methods

AIRCC-Clim is composed of four main modules: greenhouse gas emission scenario editor; global climate models, a regional scenario generator; and a climate risk index generator (Fig. 1). In the following paragraphs each module is discussed, including detailed descriptions of the modelling approaches, methods and data sources.

3.1. Emissions scenario editor

AIRCC-Clim offers a graphic interface for constructing user-defined global emissions scenarios for six climate changing substances: Fossil and industrial carbon dioxide (CO_2 in MtC/yr), methane (CH_4; in $MtCH_4$/yr), nitrous oxide (N_2O; MtN_2O–N/yr), chlorofluorocarbons (CFC_{11}, CFC_{12} in kt/yr), and sulfur hexafluoride (SF_6 in kt/yr). Four RCP emissions trajectories are included by default and the user can select one of them as starting point for editing. As shown in Fig. 2 AIRCC-Clim has three input options for global emissions: 1) by means of editing the values displayed on a table; 2) by selecting and plotting the substance of interest and modifying the emissions trajectories directly in a graph; 3) loading an Excel file (.xlsx) with user-defined emissions trajectories for each gas in a predefined format (see the AIRCC-Clim user guide included in the SI). The modified emissions scenario is saved in an Excel (.xlsx) file and used for generating the corresponding climate projections in AIRCC-Clim.

3.2. Global climate projections

Global temperature projections in AIRCC-Clim can be generated by running a simple climate model, as well as by using precalculated projections from two reduced complexity climate models. As described in the following paragraphs, in all cases probabilistic projections are

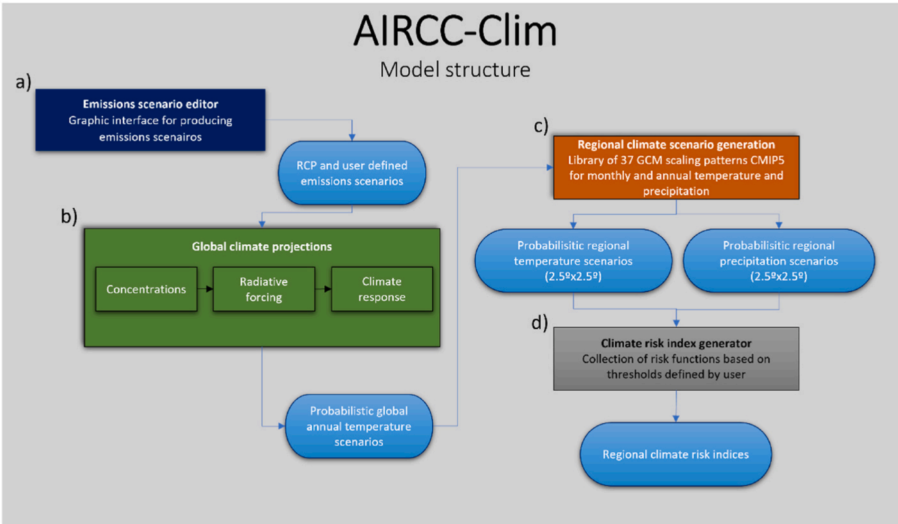

Fig. 1. Schematic representation of AIRCC-Clim model structure. Calculation modules are represented by rectangles while output is denoted by rectangles with rounded corners. The four modules are: a) the emissions scenario editor; b) the climate module which produces annual global temperature change estimates; c) the regional climate scenario generator which produces probabilistic monthly and annual climate projections, and; d) the climate risk index generator that calculates risk measures defined by the user.

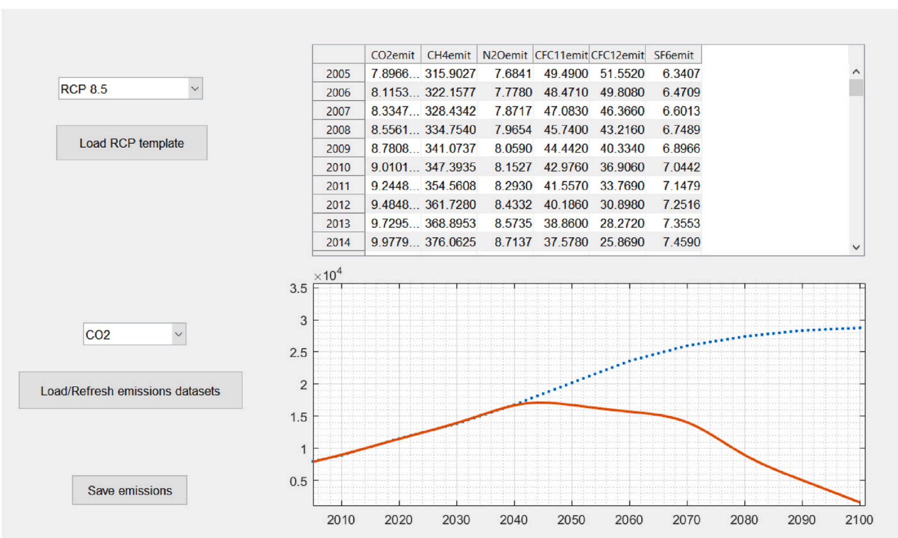

Fig. 2. AIRCC-Clim's graphic global emissions editor. Four RCP emissions trajectories can be loaded and edited by the user by means of: 1) modifying the values in the editor's table (upper part); 2) by changing the trajectory in an interactive graph (lower part) and; 3) loading an Excel file with user-defined emissions trajectories. In the lower part of the figure, the dashed blue line shows the default values for the selected RCP scenario, while the continuous red line shows the trajectory edited by the user.

constructed by means of stochastic simulation to represent uncertainty in the climate sensitivity (CS) parameter.

3.2.1. Modified schneider-thompson model

The Schneider-Thompson (ST) simple climate model (Schneider and Thompson 1981) includes three components that allows to calculate the atmospheric concentrations of greenhouse gases, the corresponding change in radiative forcing and the resulting increase in global temperature. Due to its flexibility and low computational cost, this climate model (and modified versions of it) is used in some of the most popular integrated assessment models, such as FUND and RICE (Nordhaus and Boyer 2003; Anthoff and Tol 2014a).

The version of the ST model in AIRCC-Clim builds upon that used in the FUND integrated assessment model (Tol and Fankhauser 1998) which is available at http://www.fund-model.org/. In this section, the ST model and the modifications that are introduced in AIRCC-Clim. As described below, several AIRCC-Clim's parameters are calibrated using MAGICC6 output (Meinshausen et al., 2011b), as well as the best estimates and likely ranges included in the IPCC's Fifth Assessment Report (AR5). The MAGICC6 model was calibrated with climate projections from different general circulation models included in CMIP5 (Meinshausen et al., 2011c, a).

Calculation of atmospheric concentrations and radiative forcing.

A five box-model (Maier-Reimer and Hasselmann 1987; Tol 2019a) is used to convert annual emissions of CO_2 (MtC) into atmospheric concentrations (ppm). The initial value for CO_2 concentrations is 278 ppm which represent preindustrial times (circa 1750). The carbon cycle model is represented by the following equation:

$$C_{i,t}^{CO_2} = (1-\alpha_i)C_{i,t-1}^{CO_2} + \gamma_i \beta E_t^{CO_2} \tag{1}$$

$$C_t^{CO_2} = \sum_{i=1}^{5} C_{i,t}^{CO_2} \tag{2}$$

where $C_{i,t}^{CO_2}$ represents the atmospheric concentrations of CO_2 in box $i =$ *1;,5* at time t, E_t are the CO_2 emissions at time t, α_i determines how long CO_2 remain in box i, while γ_i is the proportion of emissions that enter box i, and β is a scale parameter ($\beta = 0.00045$). The α_i and γ_i parameters are taken from the literature (Maier-Reimer and Hasselmann 1987; Hammitt et al., 1992; Tol 2019b), while the β is a calibration parameter obtained by minimizing the sum of squares of the differences between the MAGICC6 concentrations reported in (Meinshausen et al., 2011b) and those obtained from equations (1) and (2) under the RCP8.5 scenario. The CO_2 emissions in AIRCC-Clim correspond to those of fossil and industrial emissions. These boxes are characterized by different decay times that resemble the slow and fast components of the carbon cycle. However, these boxes do not represent physical processes and are just simple mathematical devices that allow to approximate the observed concentrations (Schneider and Thompson 1981; Maier-Reimer and Hasselmann 1987; Tol 2019a). $C_t^{CO_2}$ is the total concentration of CO_2 in the atmosphere at time t. Parameter values are reproduced in Table S1. We use a common parameterization for CO_2 radiative forcing (Meinshausen et al., 2011a):

$$F_t^{CO_2} = 5.35 ln\left(\frac{C_{i,t}^{CO_2}}{C_{pre}^{CO_2}}\right) \tag{3}$$

where $C_{pre}^{CO_2} = 278$ represents the preindustrial atmospheric concentrations of CO_2.

CH_4 concentrations are calculated using the following equation:

$$C_t^{CH_4} = (1 - a_1)C_{t-1}^{CH_4} + a_1 C_{pre}^{CH_4} + b_1 E_t^{CH_4} \tag{4}$$

where $C_t^{CH_4}$ are the atmospheric concentrations of CH_4 at time t, $C_{pre}^{CH_4} = 721.89$ is the preindustrial concentrations of CH_4, $E_t^{CH_4}$ are the emissions of CH_4 at time t, $a_1 = 1/12$ with 12 years representing the permanence of CH_4 in the atmosphere (Stocker et al., 2013; Anthoff and Tol 2014b) and $b_1 = 0.2954$ is a scaling factor and was obtained by minimizing the sum of squared differences between the MAGICC6 concentrations and those obtained from equation (4) under the RCP8.5 scenario.

The atmospheric concentrations of N_2O are calculated using an equation similar to that of CH_4:

$$C_t^{N_2O} = (1 - a_2)C_{t-1}^{N_2O} + a_2 C_{pre}^{N_2O} + b_2 E_t^{N_2O} \tag{5}$$

where the emissions and atmospheric concentrations of N_2O are denoted by $E_t^{N_2O}$ and $C_t^{N_2O}$, respectively, while $C_{pre}^{N_2O} = 272.96$, $a_2 = 1/120$, with 120 years representing the persistence of the gas in the atmosphere (Stocker et al., 2013; Tol 2019b), and $b_2 = 0.1550$, obtained by minimizing the sum of squared differences between the MAGICC6 concentrations and those obtained from equation (4) under the RCP8.5 scenario.

Calculating the radiative forcing of CH_4 and N_2O involves an interaction term between these gases to account for their overlap in the absorption bands as represented in the following equations:

$$Int_t^{CH_4} = f(M, N_0) - f(M_0, N_0) \tag{6}$$

$$Int_t^{N_2O} = f(M_0, N) - f(M_0, N_0)' \tag{7}$$

where these interaction functions are given by:

$$f(M, N_0) = p_1 ln\left[1 + p_2\left(C_t^{CH_4} C_{t=0}^{N_2O}\right)^{0.75} + p_3 C_t^{CH_4}\left(C_t^{CH_4} C_{t=0}^{N_2O}\right)^{1.52}\right] \tag{8}$$

$$f(M_0, N) = p_1 ln\left[1 + p_2\left(C_{t=0}^{CH_4} C_t^{N_2O}\right)^{0.75} + p_3 C_t^{CH_4}\left(C_{t=0}^{CH_4} C_t^{N_2O}\right)^{1.52}\right] \tag{9}$$

$$f(M_0, N_0) = p_1 ln\left[1 + p_2\left(C_{pre}^{CH_4} C_{t=0}^{N_2O}\right)^{0.75} + p_3 C_{pre}^{CH_4}\left(C_{pre}^{CH_4} C_{t=0}^{N_2O}\right)^{1.52}\right] \tag{10}$$

$$f(M_0, N_0)' = p_1 ln\left[1 + p_2\left(C_{t=0}^{CH_4} C_{pre}^{N_2O}\right)^{0.75} + p_3 C_{pre}^{N_2O}\left(C_{t=0}^{CH_4} C_{pre}^{N_2O}\right)^{1.52}\right] \tag{11}$$

with $p_1 = 0.47$, $p_2 = 2.01*10^{-5}$, $p_3 = 5.31*10^{-15}$ (Ramaswamy et al., 2001; Anthoff and Tol 2014b; Tol 2019b). The radiative forcing of CH_4 and N_20 is calculated as:

$$F_t^{CH_4} = 0.036\left[\left(C_t^{CH_4}\right)^{0.5} - \left(C_{pre}^{CH_4}\right)^{0.5}\right] - Int_t^{CH_4} \tag{12}$$

$$F_t^{N_2O} = 0.12\left[\left(C_t^{N_2O}\right)^{0.5} - \left(C_{pre}^{N_2O}\right)^{0.5}\right] - Int_t^{N_2O} \tag{13}$$

CFC_{11} and CFC_{12} concentrations are calculated as follows:

$$C_t^{CFC_{11}} = (1 - a_3)C_{t-1}^{CFC_{11}} + b_3 E_t^{CFC_{11}} \tag{14}$$

$$C_t^{CFC_{12}} = (1 - a_4)C_{t-1}^{CFC_{12}} + b_4 E_t^{CFC_{12}} \tag{15}$$

In which a_3 and a_4 are equal to 1/45 and 1/100, with 45 and 100 years representing the permanence of CFC_{11} and CFC_{12} in the atmosphere (Stocker et al., 2013; Tol 2019b), while $b_3 = 0.0423$ and $b_4 = 0.0481$ were obtained by minimizing the sum of squared differences between the MAGICC concentrations reported in (Meinshausen et al., 2011b) and those obtained from equations (14) and (15) under the RCP8.5 scenario, respectively. The radiative forcing from CFCs is calculated by multiplying it by a scaling factor equal to 0.25/1000 in the case of CFC_{11} and 0.32/1000 for CFC_{12} (Ramaswamy et al., 2001; Anthoff and Tol 2014b; Tol 2019b).

Finally, the concentrations of SF_6 are obtained using the following equation:

$$C_t^{SF_6} = (1 - a_5)C_{t-1}^{SF_6} + a_5 C_{pre}^{SF_6} + b_5 E_t^{SF_6} \tag{16}$$

where $a_5 = 1/3200$, with 3200 years as the permanence of SF_6 in the atmosphere (Forster et al., 2007), and $b_5 = 0.0393$ was obtained by minimizing the sum of squared differences between the MAGICC concentrations and those obtained from equation (16) under the RCP8.5 scenario. The radiative forcing of SF_6 is calculated as $F_t^{SF_6} = 0.00052^* C_t^{SF_6}$ (Ramaswamy et al., 2001; Tol 2019b).

As shown in Fig. S1, the equations and parameterizations used for calculating the concentrations and radiative forcings from the greenhouse gases included in AIRCC-Clim can closely approximate those produced with MAGICC6. In all cases, the goodness of fit from running a regression between the output from AIRCC-Clim and MAGICC6 under the RCP8.5 scenario produces R^2 values larger than 0.99 (Fig. S1). Fig. S2 shows the AIRCC-Clim and MAGICC6 concentrations and radiative forcing for the RCP8.5, RCP6, RCP4.5 and RCP2.6 for individual greenhouse gases and for the sum of their radiative forcing. The average differences in the sum of radiative forcing from the AIRCC-Clim and MAGICC6 output are 2%, 7%, 6%, 7% for the RCP8.5, RCP6, RCP4.5 and RCP2.6, respectively.

Calculation of global temperature change.

The ST model uses the following two interlinked equations to produce annual mean global air and ocean surface temperatures:

$$T_t^A = T_{t-1}^A + \lambda_1\left(\lambda_2 F_t - T_{t-1}^A\right) + \lambda_3\left(T_{t-1}^O - T_{t-1}^A\right) \tag{17}$$

$$T_t^O = T_{t-1}^O + \lambda_4\left(T_{t-1}^A - T_{t-1}^O\right) \tag{18}$$

Following Tol (2019a) we use the following parameter values as the initial calibration: $\lambda_1 = 0.0256$, $\lambda_2 = 1.14891$, $\lambda_3 = 0.00738$, and $\lambda_4 = 0.00568$. The CS of this model is calculated as $\lambda_2[5.35\ln(2)]$ and it is the main parameter for calibrating the model to reproduce observed or projected annual mean global air surface temperature. A limitation with this approach is that the accuracy of its projections will depend on which temperature series is used for calibration. To illustrate this, we use the projections obtained from the MAGICC6 model for the RCP8.5, RCP6, RCP4.5 and RCP2.6 for the period 2005–2100. These simulations are obtained using the total radiative forcing factors, not only the 6 gases described above. For parameter calibration, the temperature change projections of the ST model are calculated using the same total radiative forcing used to produce those of MAGICC6. The calibration procedure used was to minimize the sum of the squared residuals between the ST and the MAGICC6 projections using ordinary least squares. The optimal CS values that calculated for each scenario are 3.27 (RCP8.5), 2.70 (RCP6), 2.64 (RCP4.5) and 2.23 (RCP2.6). Choosing any single value of this parameter to project all the RCP scenarios would lead to over- or underestimating future temperatures, particularly in the case of extreme scenarios (RCP2.6 and RCP8.5). As such, this approach could have an impact on, for example, the evaluation of the benefits of mitigation policies.

The level of warming is closely related to the total cumulative emissions of CO_2 (TCRE; Fig. S3). The relationship between global temperature change and TCRE is relatively constant over time and independent from the emissions scenario used, but it is dependent on the global climate model CS and transient climate response (Collins et al., 2013). Fig. S3 shows the differences in the temperature change projections of MAGICC6 and the ST as a function of total cumulative emissions of CO_2 from different RCP scenarios. In this figure, the ST projections are shown for when the CS is fixed and calibrated for a particular RCP and for when the CS is allowed to vary across RCP scenarios. When the CS is calibrated using one of the RCP scenarios and it is used for projecting temperature change for the other RCP scenarios, the differences between the ST and the MAGICC6 projections can be as large as 1.55 °C. These differences are much smaller when the CS value is allowed to change for different RCPs (the mean and maximum differences are 0.02 °C and 0.17 °C, respectively), which suggest that the emulating capacity of the ST model could be greatly improved if the CS value is allowed to vary across cumulative emissions. Simple climate models such as ST are based on extremely stylized representations of the climate system and necessarily ignore several relevant aspects of, for example, climate feedbacks and other processes that determine the responses to changes in external forcing and, thus, the CS. While the CS in the climate system and in complex climate models is an emergent property, in reduced complexity climate models is a parameter to be calibrated. The ST ignores many climate feedbacks and other radiatively active compounds, which also contributes to the differences in temperature projections obtained with MAGICC6. A sensible calibration of the CS can help compensate the omissions in simple models and increase their ability to reproduce the output of more complex models. We stress that the CS specification in AIRCC-Clim is as a useful device for approximating more closely temperature change projections for the range of RCPs projections, but that the parameterization of the CS should not be interpreted as a physical statement about how the climate system operates.

Fig. 3 shows a linear relationship between cumulative CO_2 emissions and the CS value the ST model requires to better approximate the temperature change projections from MAGICC6. Given this relationship, we propose a dynamic CS parameter for the ST model that is calculated based on the cumulative CO_2 emissions, which are dominant in any RCP, SRES or other realistic emissions scenario. The proposed parameterization for the CS has the practical purpose of increasing the emulation capacity of the ST model and to fully exploit the ability of simple models to approximate the results from much more complex ones with only a small fraction of computing effort. While the proposed dynamic CS is only a practical device to increase the emulation capacity of the model, there is increasing evidence that the climate system's feedbacks are dependent on forcing magnitudes and timescales and thus the CS may be not a constant value, both in reality as in complex climate models (Knutti and Rugenstein 2015).

In the proposed dynamic CS, this parameter is calculated prior to projecting global temperatures with the ST model. The regression equation that relates the CS and the cumulative CO_2 emissions is $CS = 2.05 + 6.18 \times 10^{-7} \sum CO_2$ ($R^2 = 0.96$; Fig. 3). To get a better approximation for the lowest and highest cumulative scenarios, we also fitted a line based on the CS values for RCP2.6 and the RCP8.5. The results were compared to the projections in the IPCC's AR5 and were optimized to reproduce the best estimates (Stocker et al., 2013). The final extreme CS values are 2.1 °C and 3.3 °C for the RCP2.6 and RCP8.5 scenarios, respectively. The final equation relating CS and cumulative CO_2 emissions is

$$CS = 1.85 + 7.51 \times 10^{-7} \sum CO_2 \tag{19}$$

The CS values are restricted to the interval [2.1, 3.3]. Table 1 shows the projections of the modified ST model and the best estimates and likely ranges in the AR5 (Collins et al., 2013). For all four RCP emissions scenarios and both short- and long-term horizons, the average difference is about 0.08 °C and the maximum 0.23 °C. This illustrates that the modified ST model very closely resembles the IPCC AR5 temperature projections. The differences in projections between MAGICC6 and AIRCC-Clim are, in part, due to the omission of other radiative active compounds, as the latter only considers 6 greenhouse gases. The differences in the 2046–2065 horizon are slightly larger and may be related to the omission of aerosols and land use CO_2 emissions which have a more significant influence in the shorter-term.

To extend the ST model to account for the uncertainty in CS values and to produce probabilistic projections, we represent the model's CS with a triangular distribution. The model output of global temperature change projections is affected by the distribution chosen for the CS parameter. Our choice to represent the CS with a triangular distribution is common in the integrated assessment literature such as in the PAGE and CLIMRISK models (Moore et al., 2018; Estrada and Botzen 2021). Note that other probability distributions and parameterizations could be used to explore different assumptions about the CS (Gay and Estrada

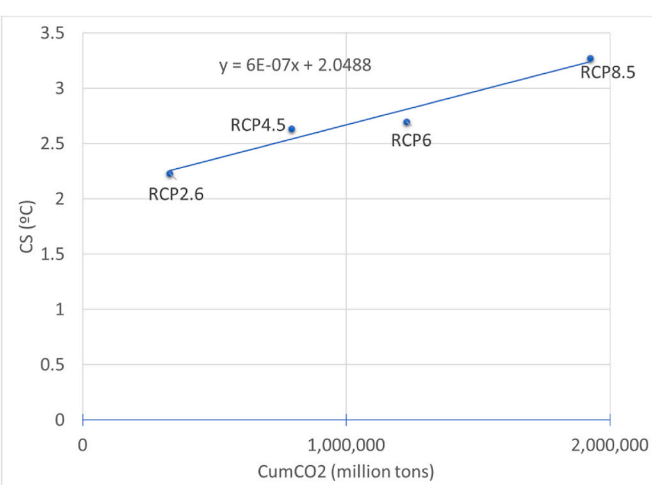

Fig. 3. Scatter plot between cumulative CO_2 emissions and the climate sensitivity that minimizes the sum of squared errors between the TS and the MAGICC6 projections.

Table 1
Comparison between the projected change in global mean surface air temperature for the mid- and late 21st century (with respect to preindustrial times) reported in the IPCC's AR5 and those obtained with the modified ST model.

		2046–2065		2081–2100	
		Mean	Likely range	Mean	Likely range
RCP2.6	IPCC	1.61	1.01–2.21	1.61	0.91–2.31
	ST*	1.56	1.06–2.10	1.67	*1.10–2.31*
RCP4.5	IPCC	2.01	1.51–2.61	2.41	1.71–3.21
	ST*	1.94	1.39–2.54	2.44	*1.70–3.25*
RCP6	IPCC	1.91	1.41–2.41	2.81	2.01–3.71
	ST*	2.15	1.59–2.75	3.01	*2.17–3.92*
RCP85	IPCC	2.61	2.01–3.21	4.31	3.21–5.41
	ST*	2.80	2.17–3.48	4.32	*3.30–5.43*

Note: Table 1 is taken from the IPCC's AR5 Working Group I report (Table 12.2 in Collins et al., 2013). The values in such table are calculated with respect to 1986–2005. According to footnote a), the warming from preindustrial times (1850–1900) to 1986–2005 is 0.61 °C. To obtain the values for the preindustrial reference period, 0.61 °C was added to every entry on Table SPM12.2 of the IPCC's AR5.

2010). In this distribution the most likely value is given by equation (19) above, and the lower and upper limits are the calculated CS value plus/minus some constants that are to be calibrated. The equations for the upper (CS^{high}) and lower limits (CS^{low}) of the triangular distribution for CS are:

$$CS^{low} = CS + h_1 \quad (20)$$

$$CS^{high} = CS + h_2 \quad (21)$$

The h_1 and h_2 constants are calibrated to match the likely ranges reported in the IPCC's AR5. Simulations of 10,000 realizations were used and the 5th and 95th percentiles were chosen to construct the ST likely ranges. The parameter values that provided good fit for all RCPs are $h_1 = 1.1$ and $h_2 = 1.5$. Table 1 shows that the likely ranges of the modified ST model closely reproduce those reported in the IPCC for both short- and long-term horizons, showing almost exact overlap with differences in upper and lower limits typically smaller than 0.2 °C.

3.2.2. *Generating probabilistic global temperature projections using precalculated runs from MAGICC6 and the Thermodynamic Climate Model*

The MAGICC6 and the Thermodynamic Climate Model (TCM) are reduced-complexity climate models that were designed for different objectives. MAGICC is composed of a set of coupled models that include gas cycles and climate and ice-melt models designed to explore the effects of anthropogenic emissions of greenhouse gas concentrations, radiative forcing, and changes in global mean annual temperature and sea level (Wigley 1995; Meinshausen et al., 2011c, a). The TCM was originally conceived as a weather forecast model for the northern hemisphere and then extended to the global scale for studying the climate of Earth and of other planets in the Solar System (Adem 1991). In the case of MAGICC6, precalculated projections of global temperature are included in AIRCC-Clim for the emissions scenarios RCP2.6, RCP4.5 RCP6 and RCP8.5, while in the case of the TCM the precalculated that were available are the RCP4.5, RCP6 and RCP8.5.

To account for the uncertainty in CS values and to produce probabilistic projections, we propose a simple method based on linear regression and statistical simulation. Due to the availability of climate models' output we base our calculations on MAGICC6. Projections for each RCP scenario were obtained using of MAGICC6 for three different CS values that represent medium CS (3.0 °C), low CS (1.5 °C) and high CS (4.5 °C). To emulate MAGICC's results for high and low climate sensitivities, we propose the use of some scaling weights *w* that would approximate them when multiplied by the global temperature obtained using a medium CS value. Such weights can be obtained by means of the following regression:

$$T_t^{sens^*} = \omega T_t^{medium} + \varepsilon_t \quad (22)$$

where $T_t^{sens^*}$ is the global temperature projection obtained with MAGICC6 using either low or high CS, while T_t^{medium} corresponds to the global temperature projection obtained with medium CS; ω is the slope parameter and ε_t are the regression residuals. In all cases, the R^2 is higher than 0.99; note that the objective of these models is not to make inference about parameter values, but just to produce a close fit of projections using different values of CS. The values of parameter ω for the different combinations of CS and for each RCP emissions scenario are provided in Table 2. The estimated parameter values are very similar for different RCPs with an average value of 1.34 and 0.57 for high and low CS values, respectively. As shown in Fig. 4, these values allow to closely approximate the simulations of MAGICC6 produced using high/low CS values by scaling a simulation of the same model calculated with medium sensitivity. The approximation is less precise when used on scenarios that lead to stabilization (Fig. 4d), but the error is still very small (0.17 °C for the high CS projection using the RCP2.6).

Table 2
Estimated slope parameter values of regression $T_t^{sens^*} = \omega T_t^{medium} + \varepsilon_t$ for annual mean air surface global temperature projections using MAGICC6.

Scenario	ω (CS = 4.5)	ω (CS = 1.5)
RCP8.5	1.3369	0.5762
RCP6	1.3345	0.5720
RCP4.5	1.3430	0.5652
RCP3PD	1.3510	0.5582
Mean	1.3414	0.5679

To produce probabilistic scenarios using the ST model, we use a triangular distribution to scale the MAGICC6 runs obtained with a medium CS. The parameters of the triangular distribution are 1 for the mode or most likely value and, 0.5679 and 1.3414 for the lower and upper limits, respectively (Table 2). These parameter values allow to emulate the projections that would be obtained with MAGICC6 randomly choosing CS values contained in the interval 1.5 °C to 4.5 °C, assigning a larger probability of occurrence to values that are closer to the medium sensitivity of 3 °C. CS is high uncertainty (Rogelj et al., 2014; Lewis and Curry 2015; Freeman et al., 2015; Tan et al., 2016; Friedrich et al., 2016; Knutti et al., 2017; Cox et al., 2018). However, the consensus is that the CS is probably within the 1.5 °C to 4.5 °C interval with a central estimate of 3 °C (Bony et al., 2013; Callendar, 1938; Freeman et al., 2015; Santer et al., 2019; Stocker et al., 2013). This CS range encompasses the range produced by the state-of-the-art models included in the CMIP5 (Jonko et al., 2018; Stocker et al., 2013).

Given that in the TCM the CS is not an explicit parameter as in MAGICC6, but an emerging property of the model, there are no high/low CS projections that can be used to find the corresponding parameters in Table 2. As such, we apply the same scaling parameters we found for MAGICC6 to represent uncertainty in CS values and to extend the TCM projections to be probabilistic.

3.3. *Regional climate projections*

Pattern scaling is a technique for producing regional scenarios based on the robust finding documented in the literature of stationarity in geographical patterns of change in some climate variables, in particular temperature and precipitation (Santer et al., 1990; Collins et al., 2013; Tebaldi and Arblaster 2014). These patterns can be scaled by global temperature change to produce regional climate change scenarios in a simple and computationally efficient manner that provide a useful approximation to those produced by complex global climate models.

The performance of pattern scaling techniques has been evaluated in the literature in several occasions (Mitchell 2003; Cabré et al., 2010; Collins et al., 2013; Tebaldi and Arblaster 2014; Herger et al., 2015; Kravitz et al., 2017a; Zelazowski et al., 2018; Tebaldi and Knutti, 2018; Osborn et al., 2018). These techniques produce adequate approximations for variables such as annual/seasonal temperature and precipitation and other variables excluding extreme events and time-scales in which natural variability is dominant. These patterns are also adequate for most of the emissions scenarios, including low-warming policy trajectories and most regions except where local forcing is strong and time-varying (Collins et al., 2013; Estrada and Botzen 2021). An example of the latter are scenarios that involve very high aerosols emissions. The reason is that the modelling approach does not capture the effects of regional cooling by aerosols or land-surface feedbacks due to conditions that not reflected by the library of scaling patterns.The pattern scaling technique can be described as follows (Collins et al., 2013; Tebaldi and Arblaster 2014; Estrada and Botzen 2021):

$$P(i,j,t,E,y,s) = T(t,E)p(i,j,y,s) + \xi(i,j,t,s) \quad (23)$$

where i, j denote longitude and latitude, respectively, and t is time. E represents the emissions scenario, y is the climate variable of interest, s is the time of the year for which the scenarios is constructed (annual, month, season) and $T(t)$ is the global annual mean temperature change

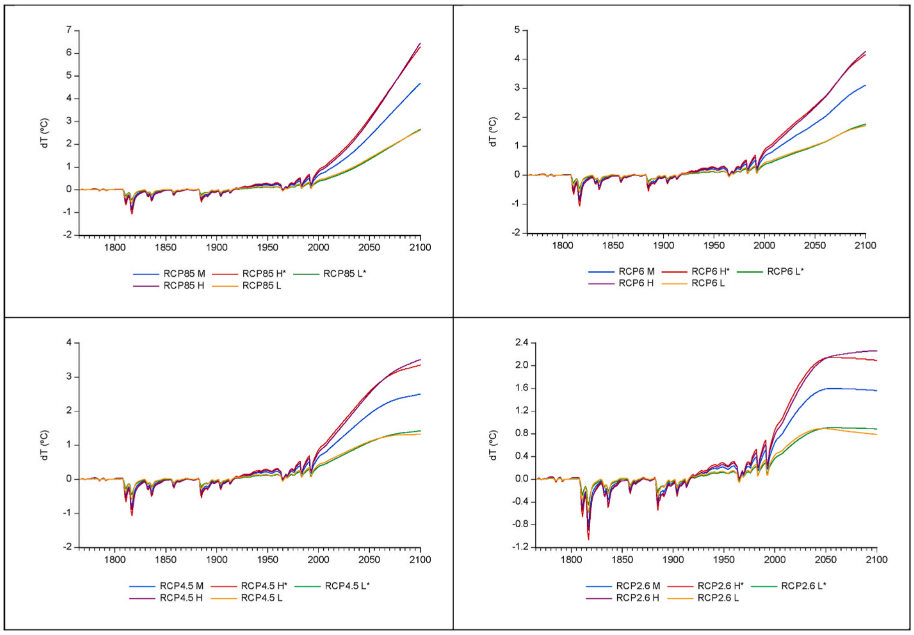

Fig. 4. Actual MAGICC6 projections for different RCP scenarios and projections of high/low CS approximated using the parameters in Table 2. M, H, L denote projections using medium, high, and low CS values, while the symbol * indicates the projections are obtained using the average scaling parameters in Table 2.

at time t under the emission scenario E. $P(\cdot)$ is the projected field of change for variable y obtained using a complex climate model, while $p(\cdot)$ is the time/emissions scenario invariant spatial pattern of change per 1 °C change in annual global mean temperature, for the climate variable y. $\xi(i,j,t,s)$ represents is an error term due to both natural variability and the limitations of the pattern scaling methodology (Collins et al., 2013; Estrada and Botzen 2021).

The patterns $p(i,j,y,s)$ were calculated for monthly and annual air surface temperature and precipitation using simulations from a battery of coupled ocean-atmosphere general circulation models (Table S2) under the RCP8.5 emissions scenario and that are available at the CMIP5 data portal (https://esgf-node.llnl.gov/search/cmip5/). All simulations were bilinearly interpolated into a common grid with a spatial resolution of 2.5° × 2.5°. The Hodrick Prescott filter (Hodrick and Prescott 1997) was applied to the time series from each grid point from the climate models' simulations to remove the effects of high frequency variability. Then, temperature/precipitation time series from each grid cell were regressed on the global mean temperature and the slope coefficients were stored as maps that represent the scaling patterns (Kravitz et al., 2017b; Lynch et al., 2017). For producing the regional climate change scenarios, global mean temperature projections from section 2.2 are used to scale the patterns produced in this section. The projections are expressed in °C for changes in temperatures and in percentage of change for precipitation, with respect to preindustrial conditions (c. 1750). AIRCC-Clim allows the user to select the scaling patters for any given climate model, as well as to generate probabilistic scenarios combining all of them. This stochastic version of AIRCC-Clim uses a uniform distribution which assigns the same probability to each of the climate models. A variety of approaches for assigning probabilities to climate models' output have been proposed in the literature (Xu et al., 2010; Knutti et al., 2010; Mendlik and Gobiet 2016) but there is no agreement on which would be the best way of doing it (Knutti 2010; Stephenson et al., 2012; Deser et al., 2014; Notz 2015). The uniform distribution follows the Principle of Insufficient Reason which is the maximum entropy distribution in absence of any additional information (Jaynes 1957; Jaynes et al., 2003; Gay and Estrada 2010). Other probability distributions based on performance evaluation or model dependence could be implemented, however these distributions may be as arbitrary as assigning equal probabilities to each model and may lead to unjustified dismissal of uncertainty (Potter and Colman 2003; Gay and Estrada 2010; Altamirano del Altamirano del Carmen et al., 2021).

Climate change scenarios for temperature and precipitation can be exported as GeoTIFF and netCDF files for three time horizons: 2030 (2021–2040), 2050 (2041–2060) and 2070 (2061–2080). Maps of changes in temperature and precipitation for any year between 2005 and 2100 can be exported as high-quality PNG and as netCDF files.

3.4. Climate risk index generator

AIRCC-Clim uses the probabilistic nature of its projections to produce user-defined risk measures based on thresholds. The current version of the model includes two types of risk metrics: probabilities of exceedance and the dates when the selected threshold is exceeded. The threshold values are selected by the user to reflect his perceptions of risk and information needs. Note that due to the exporting capabilities of this software, AIRCC-Clim's output can be combined with information external from the model, such as population projections to indicate hotspots of severe climate change in populated areas.

The calculation of the risks indices is done following the same procedure as CLIMRISK (Estrada and Botzen 2021). First, the indicator function is used to identify in which simulations and grid cells the threshold is exceeded. In the case of changes in temperature T, we have:

$$IRT_{i,j,t,sim} = I\left(T_{i,j,t,sim} > T^{*}\right) \quad 24$$

where $IRT_{i,j,t,sim}$ is a four-dimensional matrix in which i,j are the longitude and the latitude that define the location of the gird cell, t is time, sim is the number that identifies each of the realizations of the simulation experiment, and T^{*} is the user-defined threshold in °C. For cases in which the threshold T^{*} is exceeded the indicator function returns a value of 1 and zero otherwise. In the case of the change in precipitation P, the threshold of interest P^{*} can be positive or negative and thus the indicator function is applied as follows:

$$IRP_{i,j,t,sim} = \begin{cases} I\left(P_{i,j,t,sim} > P^{*}\right) \; if \; P^{*} > 0 \\ I\left(P_{i,j,t,sim} < P^{*}\right) \; otherwise \end{cases} \quad (25)$$

$IRP_{i,j,t,sim}$ is a four-dimensional matrix defines as above in which the indicator function returns a value of 1 if the threshold P^{*} is exceeded and zero otherwise.

Estimates of the probabilities of exceeding the thresholds T^* and P^* can be obtained by summing over the *sim* dimension:

$$PIRT_{i,j,t} = P(T_{i,j,t} > T^*) = \frac{\sum_{sim=1}^{n} IRT_{i,j,t,sim}}{n} \tag{26}$$

$$PIRP_{i,j,t} = P(P_{i,j,t} > P^*) = \frac{\sum_{sim=1}^{n} IRP_{i,j,t,sim}}{n} \text{ if } P^* > 0 \tag{27a}$$

$$PIRP_{i,j,t} = P(P_{i,j,t} < P^*) = \frac{\sum_{sim=1}^{n} IRP_{i,j,t,sim}}{n} \text{ if } P^* \leq 0 \tag{27b}$$

where $PIRT_{i,j,t}$ and $PIRP_{i,j,t}$, are three-dimensional matrices containing probability estimates. The estimated probability maps can be exported as PNG and netCDF files for any year in the period 2005–2100.

These probability estimates of exceeding critical thresholds are used to estimate the expected dates when such thresholds would be attained. These dates can be computed as follows:

$$IDT_{i,j,t} = I(PIRT_{i,j,t} \geq \gamma) \tag{28}$$

$$IDP_{i,j,t} = I(PIRP_{i,j,t} \geq \gamma) \tag{29}$$

where the parameter γ represents the percentage of simulations that is required by the user to declare the threshold has been exceeded. $IDT_{i,j,t}$ and $IDP_{i,j,t}$ are matrices in which the entries take the value 1 if the confidence level γ is attained or exceeded and zero otherwise. In AIRCC-Clim and CLIMRISK, this value is called *confidence level* and can vary with the risk tolerance of different users. The default value in AIRCC-Clim is 50%. The estimated dates for exceeding the risk threshold are obtained by mapping into a year index the first occurrence of the value 1 in the time dimension of all gird cells in $IDT_{i,j,t}$ and $IDP_{i,j,t}$. The maps of the dates of exceedance can be exported as PNG and netCDF files. Table S3 provides a list of the climate risk indices and their definition.

4. Estimating the risks of delaying the implementation of deep mitigation efforts

In this section we provide an example application of AIRCC-Clim in which the effects on climate from a high-emissions trajectory (RCP6.0) are compared to those of a deep mitigation scenario (RCP2.6) consistent

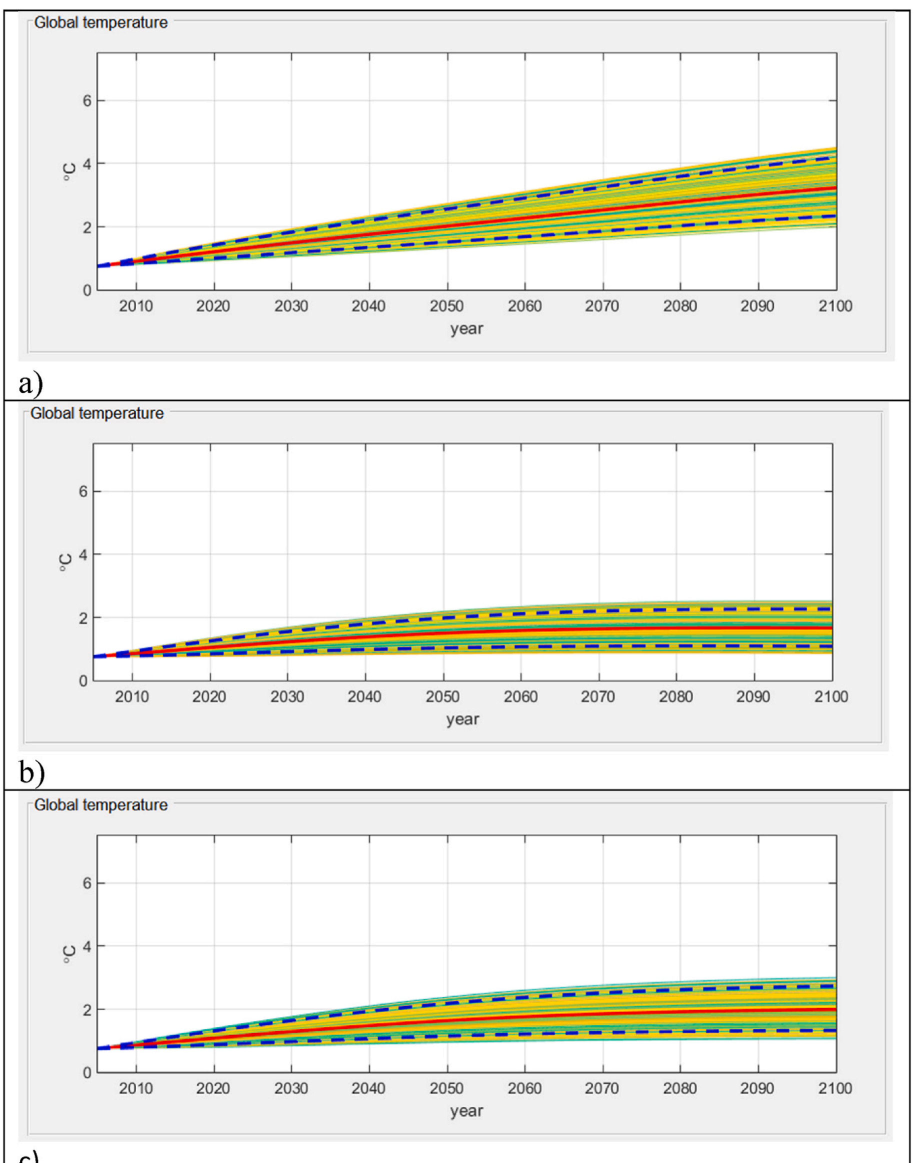

Fig. 5. Global temperature projections using the ST model. Panels a), b) and c) show the simulations for the RCP6.0, RCP2.6 and the modified RCP2.6 scenarios, respectively. The red bold line shows the mean of the ensemble while the dark slashed blue lines depict the 5th and 95th percentiles of the ensemble, and the light green and yellow lines show the individual simulations. Each experiment has 500 simulations. Changes in global temperature are with respect to preindustrial conditions (c. 1750).

with the goals of the Paris Agreement and to those in which such mitigation effort is delayed ten years.

Figure S1 shows the trajectories of CO_2, CH_4 and N_2O for the RCP6.0, RCP2.6 and the modified version of the RCP2.6 scenarios in which mitigation is delayed for 10 years, starting in 2020. The modified version of the RCP2.6 was edited in Excel and directly loaded to AIRCC-Clim using the user-defined option for emissions scenarios. The RCP6.0 and the RCP2.6 scenarios produce contrasting results in terms of their effects on climate. While the first produces a mean increase in global temperature of about 3 °C with respect to preindustrial conditions at the end of this century, and up to 4 °C when the 95th percentile is considered, the RCP2.6 limits warming below 2 °C for the ensemble mean (about 1.7 °C), although this limit is exceeded for the 95th percentile (Fig. 5). The MAGICC model produces similar results, with a mean increase in global temperature of 3.1 °C and 1.6 °C for the end of the century under the RCP6.0 and RCP2.6 scenarios, respectively (Fig. S2). The TCM produces a considerably larger mean increase for the RCP6.0 (3.9 °C), but that still lies within the likely range of the CMIP5 experiment (Table 1). The ST simulations for the modified RCP2.6 in which the mitigation effort is delayed for 10 years, show that the mean increase in global temperature reaches 2 °C in 2100, and up to 3 °C in the 95th percentile.

Figs. 6 and 7 show the changes in annual mean temperature and total annual precipitation at the grid cell level for the three emissions scenarios and two time-horizons (2050 and 2100). Temperature increase is much larger in high latitudes of the northern hemisphere due to the Arctic Amplification phenomenon (Pithan and Mauritsen 2014), reaching about 6 °C for the mid-century and more than 8 °C in 2100, under the RCP6.0 scenario (see Figs. S3 and S4 for results using the precalculated MAGICC6 and TCM runs). Most of the continents would experience temperature increases in 2050 of about 2 °C to 3 °C and of about 4 °C to 5 °C in 2100. Apart from the Arctic region, midlatitudes in North America and in Eurasia would have the largest increases (5°C-6°C) in temperature by the end of the present century, followed by Southern Asia and the Middle East, North and South Africa, parts of the west coast of North America, Mexico and the Amazonian region and the northern part of Brazil. Large changes are also expected in precipitation under the RCP6.0 scenario, with large increases in high latitudes, the equatorial Pacific Ocean and some parts of the Middle East, and large decreases in the Mediterranean, the Caribbean, Mexico, and the southern part of the US, as well as in southern parts of Africa and America (Figs. S3 and S4). The implementation of a deep mitigation effort consistent with the goals of the Paris Agreement would significantly limit these changes in climate. Under the RCP2.6 most of the Arctic would not exceed a warming of 5 °C during this century, most continents would not exceed 3.5 °C, and precipitation change would be notably smaller.

AIRCC-Clim portraits the risks of climate change, and the benefits of mitigation, in a clearer way due to its probabilistic nature and its capacity to produce maps of probabilities and of dates of exceedance. Figs. 8 and 9 show the probabilities of exceeding a 2.5 °C increase in annual temperatures and a decrease of 15% in annual precipitation in 2050 and 2100. Under the RCP6.0, by 2050 the probabilities of exceeding 2.5 °C increase in annual temperatures are higher than 60% for most of the continents, while the Arctic region and the high latitudes of the northern hemisphere are virtually certain to exceed this threshold by mid-century (Fig. S5). These simulations also show that a 2.5 °C warming would be exceeded in all continents by 2100 and that there is a high probability (above 60%) that this threshold would be crossed in all oceans, except for parts of the southern hemisphere and the Atlantic. The probabilities of exceeding a decrease of 15% in total annual precipitation in 2050 are higher than 50% for several areas of the world such as the Mediterranean, parts of Northern, Western and Southern Africa, the Caribbean and Mexico (Fig. S5). For 2100, these probabilities increase to more than 60% in those regions and extend to parts of South America and West Australia. If the emissions trajectory described in by the RCP2.6 is achieved, by 2050 the probability of exceeding 2.5 °C would be lower than 40% over the continents, except for the Arctic and parts of the midlatitudes in the northern hemisphere where the probabilities range from 60% to 100% (Fig. 8). Likewise, the probabilities of exceeding decreases in precipitation of at least 15% are considerably smaller in comparison to the RCP6.0. However, by the end of this century the probabilities of exceeding this threshold would be close to 50% for the southern region of Spain, parts of North and West Africa

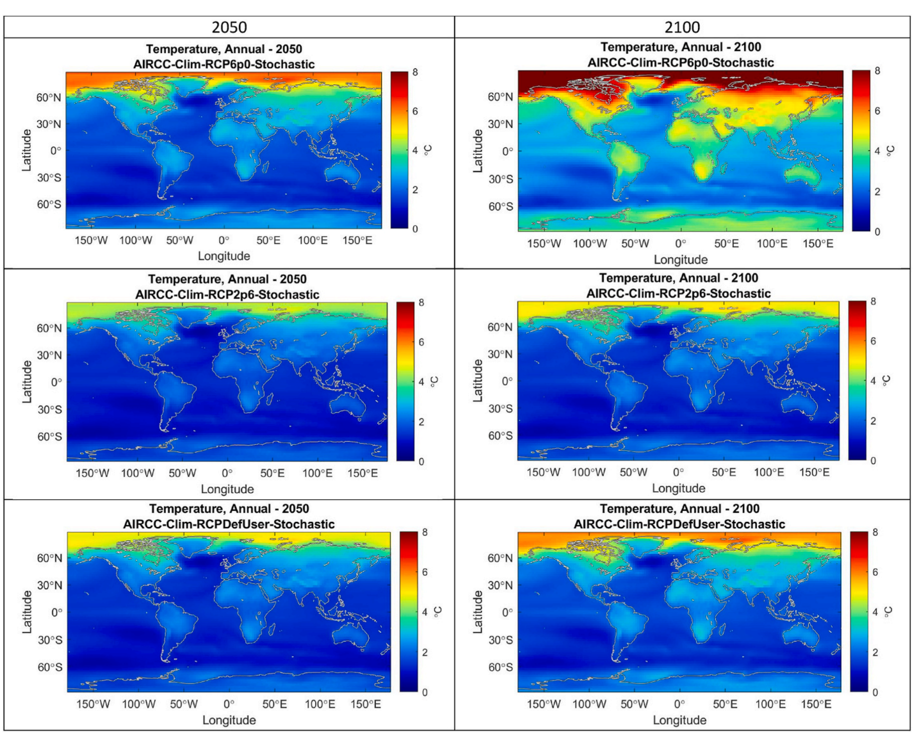

Fig. 6. Annual temperature change projections (°C) for different emissions scenarios estimated by the modified ST model. The upper panel shows the changes in temperature under the RCP6.0 scenario for 2050 (left) and 2100 (right). The middle panel shows the changes in temperature under the RCP2.6 scenario for 2050 (left) and 2100 (right). The lower panel shows the changes in temperature under the delayed RCP2.6 scenario for 2050 (left) and 2100 (right). Changes in regional temperatures are with respect to preindustrial conditions (c. 1750).

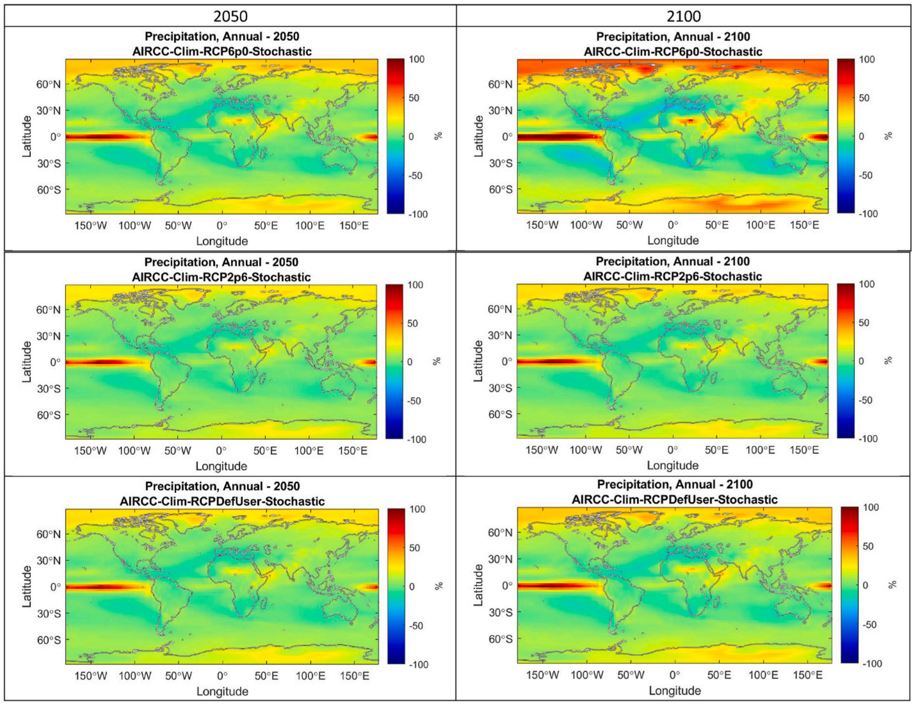

Fig. 7. As in Fig. 6 but for annual precipitation change (%).

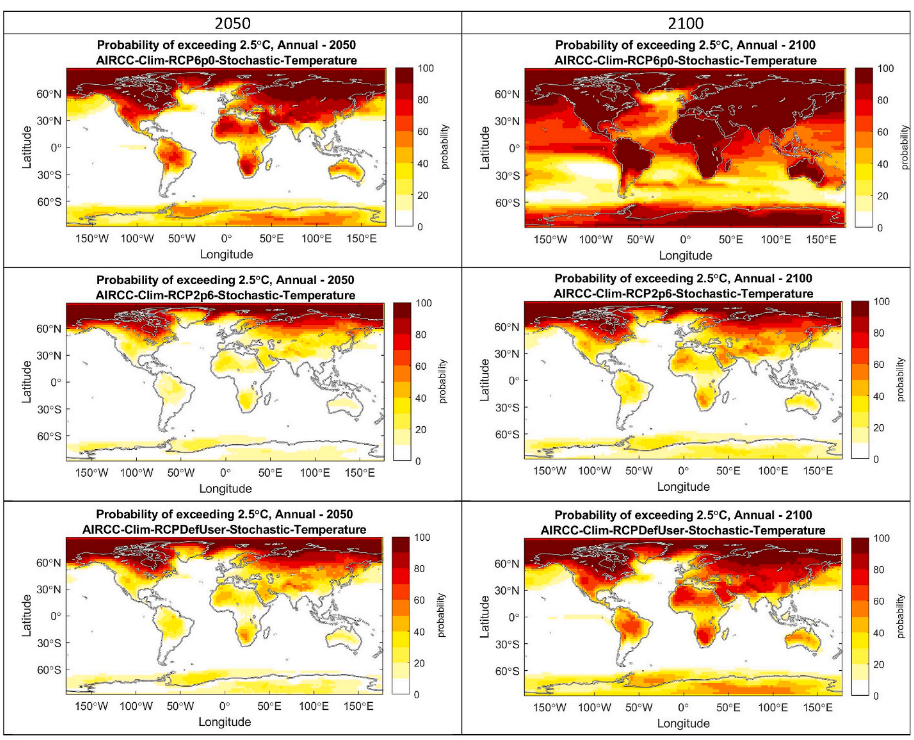

Fig. 8. Probabilities of exceeding increases of 2.5 °C in annual temperature for different emissions scenarios estimated by the modified ST model. The upper panel shows the probabilities of exceedance for the RCP6.0 scenario in 2050 (left) and 2100 (right). The middle panel shows the probabilities of exceedance for the RCP2.6 scenario for 2050 (left) and 2100 (right). The lower panel shows the probabilities of exceedance for the delayed RCP2.6 scenario for 2050 (left) and 2100 (right). Probabilities are expressed in percentages. Changes in regional temperatures are with respect to preindustrial conditions (c. 1750).

(Morocco, Mauritania, Mali, Senegal, Sierra Leone and Guinea), and about 40% for parts of the Caribbean, Central and South America (Colombia and Venezuela; Fig. 9).

Fig. 10 shows the dates when the 2.5 °C threshold would be exceeded. The default confidence level ($\gamma = 50$) was used for the estimates presented in this section. The results show that under the RCP6.0, most of the planet except for part of the southern oceans and part of the North Atlantic, would exceed the 2.5 °C threshold during this century and that some parts of the world already exceeded it (Fig. S5). The date of exceedance for the Arctic occurred during the 2000s, while for much of the high latitudes in the northern hemisphere, the Middle East, parts of South Asia, and West and South Africa, the exceedance is expected to occur in the 2020s–2030s. The remainder of the continents and the Antarctic region would go over this threshold during the period 2040–2060 and most of the oceans above the 20°S would exceed the 2.5 °C threshold during this century. The regions in which reductions of

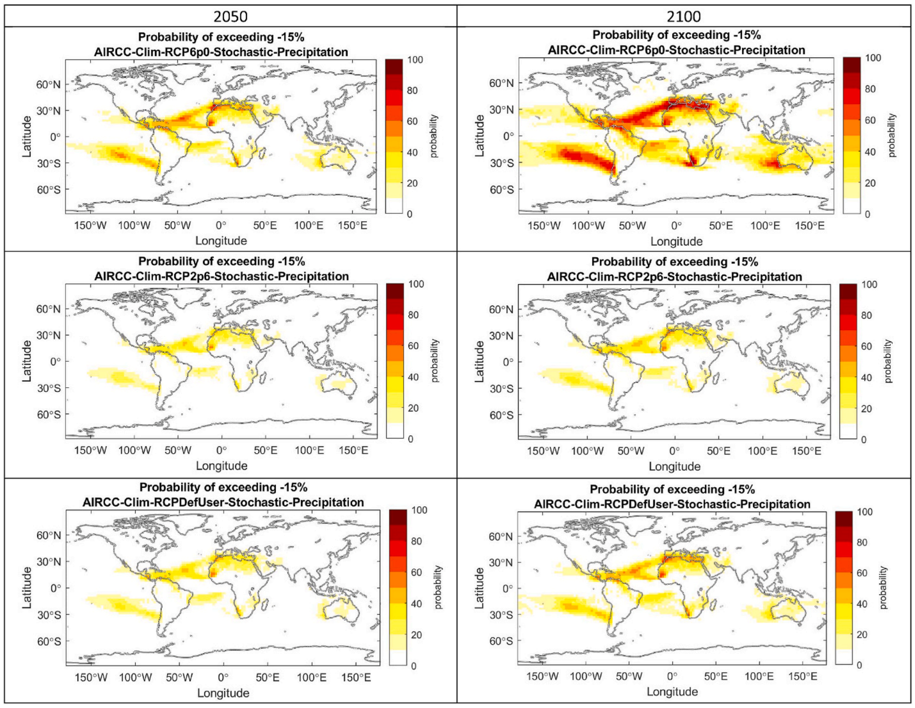

Fig. 9. As in Fig. 8 but for probabilities of exceeding decreases of 15% in annual precipitation.

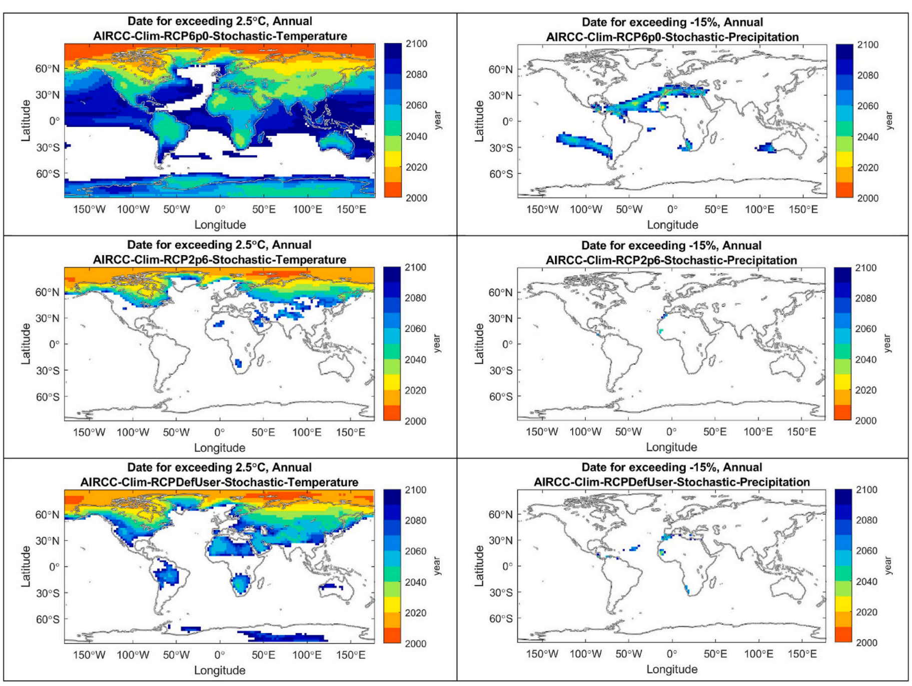

Fig. 10. Dates of exceedance for increases of 2.5 °C in annual temperature and decreases of 15% in annual precipitation for different emissions scenarios estimated by the modified ST model. The upper panel shows the dates of exceedance for annual temperature (left) and annual precipitation (right) under the RCP6.0 scenario. The middle panel shows the probabilities of exceedance for annual temperature (left) and annual precipitation (right) under the RCP2.6 scenario. The lower panel shows the probabilities of exceedance for annual temperature (left) and annual precipitation (right) under the delayed RCP2.6 scenario. Blank areas on the maps are where the projected thresholds are not exceeded at any point during the 21st century. Changes in regional temperatures and precipitation are with respect to preindustrial conditions (c. 1750).

at least 15% in annual precipitation is exceeded are fewer and form well-defined geographical patterns that cover the Mediterranean, parts of North, West and South Africa, Central America and the Caribbean, Mexico and Colombia and Venezuela in South America, as well as the west part of Australia and part of the southern Pacific Ocean (Fig. 10 and S5). The dates for exceedance on these regions are typically reached in the 2050–2060 decades, although regions of Spain and West Africa could exceed this threshold as early as the 2040s.

Achieving RCP2.6 would prevent exceeding these thresholds for most of the world during this century (Fig. 10). However, as mentioned above, some regions such as the Arctic and the high latitudes of the northern hemisphere already have exceeded the 2.5 °C temperature threshold or will do so during the next decade, regardless of the emission scenario that is selected. For parts of the midlatitudes, the RCP2.6 represents delaying reaching the 2.5 °C threshold for about 20 years, which buys time for adapting to the projected changes and to reduce risks and damages. The occurrence of this threshold would also be delayed until 2060 in some parts of the Sahara, South Africa, the Middle East and India. Exceeding decreases in precipitation of more than 15% would not occur during this century, with the exception of a few grid cells in Africa, Spain and Central America.

AIRCC-Clim runs illustrate that delaying the deep mitigation efforts of the RCP2.6 by ten years would significantly increase the risks of climate change during this century. The bottom rows of Figs. 8 and 9 show that, under delayed international action, the probabilities of exceeding 2.5 °C in annual temperature and a decrease of at least −15% annual precipitation in 2100 are similar to those obtained in 2050 for the RCP6.0 and much higher than those of the original RCP2.6. The consequences of delaying for ten years the mitigation efforts described in the RCP2.6 are clearly illustrated by Fig. 10: North and South Africa, South America, the Middle East and Central Asia would exceed a 2.5 °C increase in temperatures around 2060, when this threshold was not reached during this century under the original RCP2.6 trajectory. Parts of Australia would exceed this threshold at the end of the present century if mitigation efforts were postponed. In terms of precipitation reductions, the Mediterranean region would be most affected, as the dates of exceedance of decreases of at least 15% in precipitation would occur as soon as 2040–2050 for the south of Spain and North Africa and at the end of this century for Greece. Western Africa would go over this threshold in 2040, and parts of Central America and South Africa would see decreases of more than 15% in the 2050–2060 period. However, it is important to note that this delayed action scenario still provides important benefits in comparison with the RCP6.0, which is commonly used to represent current international mitigation commitments. Some of the most affected regions due to warming would buy time (about 2 decades) for adapting to a 2.5 °C under the delayed version of the RCP2.6. This is not so clear with regard to exceeding −15% decrease in annual precipitation for the most affected regions, as in comparison with the RCP6.0, the delayed version of the RCP2.6 would buy them only 5–10 years for implementing adaptation actions.

Monthly estimates of changes in precipitation and temperature are commonly needed for assessing the impacts of climate change in natural and human systems. AIRCC-Clim also generates estimates of monthly temperature and precipitation change, as well as estimates of probabilities and dates of exceedance for user-defined thresholds. Fig. 11 illustrates this feature for the RCP6 emissions scenario and for the central month of winter and summer (i.e., February and July). During the coldest months in the northern hemisphere's winter, the threshold of 2.5 °C was exceeded at the beginning of this century in the Arctic, while for parts of the midlatitudes it will be exceeded during this decade of in the 2030s (Fig. 11a). In most of the remaining parts of the northern hemisphere the 2.5 °C threshold in temperatures during February would be exceeded in the 2030–2050 decades. For parts of North and Central America, the driest months occur in winter and precipitation in February in those areas would decrease at least 15% as soon as 2030. In the case of regions in southern hemisphere, such as Australia, Central and South Africa, as well as most of South America, the temperature threshold during one of the hottest months (February) would occur before 2060 and, in some parts of these region, this threshold could be exceeded 20 years earlier.

The hottest months in the northern hemisphere occur during the boreal summer. As shown in Fig. 11c, exceeding the threshold a 2.5 °C increase in July would happen in this decade for regions in the Mediterranean such as Spain, France, Italy, Greece, and parts of North Africa. In these regions, exceeding this threshold in temperatures during July would be accompanied by decreases of at least 15% in precipitation before 2050 in the same month, which is one of the driest in the Mediterranean.

Moreover, due to its capabilities for exporting output, AIRCC-Clim can be easily combined with other products to address the user's specific information needs. Fig. 12 combines external population projections from the SSP3 scenario that were obtained from the CLIMRISK model (Estrada and Botzen 2021) with two risk measures produced with AIRCC-Clim to provide a first approximation of risk and exposure. Climate and population projections show that by 2050 some regions of the world will have high exposure and high probabilities of experiencing large changes in climate. In the bivariate map shown in Fig. 12a dark magenta color indicate regions for which large population and high probabilities of exceeding 15% decrease in precipitation are projected. These high-risk, high-exposure regions include large fractions of the Mediterranean, Central America and parts of the Middle East and South Asia. Light yellow areas indicate regions characterized by large population but low probabilities of decreases in precipitation of at least 15%. These include high latitude regions in the northern hemisphere for which most climate models' projections suggest an increase in precipitation. This combination of population and precipitation change would be found in parts of India, China, parts of central, northern and eastern Europe, northern US and Canada. Light blue regions such as Australia, large parts of Noth Africa and South America, are where decreases in precipitation of at least 15% are highly likely but where population counts are low.

Fig. 12b shows a bivariate map of population counts and the probability of exceeding 2.5 °C in annual temperature change by year 2050. Regions such as the eastern part of the US, Central America, most of Europe, India, China, the Middle East and parts of Africa are shown in dark magenta color. These regions are characterized by high

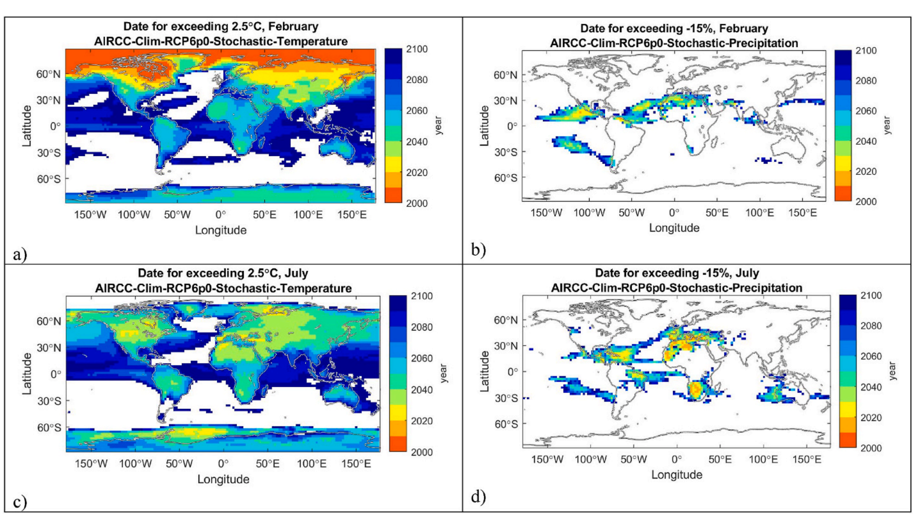

Fig. 11. Estimates of dates of exceedance during February and July for 2.5 °C and −15% thresholds in temperature and precipitation, respectively. Blank areas on the maps are where the projected thresholds are not exceeded at any point during the 21st century. Changes in regional temperatures and precipitation are with respect to preindustrial conditions (c. 1750).

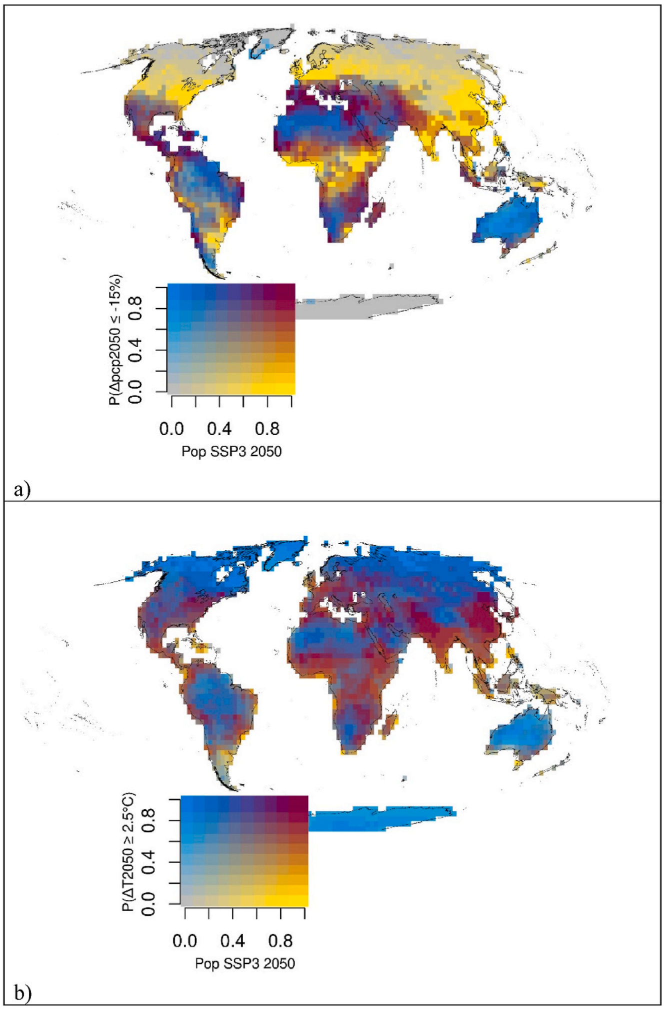

Fig. 12. Bivariate maps of population and probabilities of user-defined risk thresholds. Panel a) shows a bivariate map of population counts in year and of the probabilities of decreases in annual precipitation of at least 15% in year 2050. Panel b) shows a bivariate map of population counts and of the probabilities of warming of at least 2.5 °C in year 2050. Changes in regional temperatures and precipitation are with respect to preindustrial conditions (c. 1750).

probabilities of exceeding 2.5 °C and large population counts. Regions in light blue hue represent places where the probability of exceeding a warming of at least 2.5 °C in 2050 are high, but population in those areas is not large. This is the case of high latitudes in the northern hemisphere, Australia, the Amazon rainforest, the Sahara, Namib and the Arabian deserts. Moreover, Fig. 12 helps to identify risk hotspots in which population counts will be high in the future and significantly dryer and hotter conditions will likely occur. Such combination of factors has been associated with higher risks of human conflict and migration (Barrios et al., 2006; Hsiang et al., 2013; Hodler and Raschky 2014; World Bank 2016; Puente et al., 2016), as well as impacts on biomass production and more frequent wildfires (De Dato et al., 2008; Stevens-Rumann et al., 2018).

5. Conclusions

Here we present AIRCC-Clim, an emulator of complex climate models included in the IPCC's Fifth Assessment Report that allows generating probabilistic climate change projections and risk measures for RCP emissions scenarios, as well as for user-defined emissions scenarios. Global temperature projections are produced using a modified version of the ST model and precalculated runs of the MAGICC and TCM models. AIRCC-Clim has a spatial resolution of 2.5° × 2.5° and produces monthly and annual temperature and precipitation scenarios. This is a user-friendly, stand-alone software aimed for students, decision-makers, and researchers that allows for quick estimates of changes in climate, as well as of the probabilities and dates of exceedance of user-defined thresholds. The AIRCC-Clim model attempts to fill users' needs for models that have low technical and computing requirements, but that are able to emulate complex climate models' output and produce spatially explicit, probabilistic projections and risk measures.

AIRCC-Clim extends the ST climate model to include a dynamic climate sensitivity that takes advantage of the well-established approximately linear relationship between cumulative CO_2 emissions and global temperature increase. This extension of the ST model, combined with stochastic simulation, allows to closely approximate the best estimate and likely range included in the Fifth Assessment Report of the IPCC. By means of a simple stochastic simulation procedure, we account for the uncertainty in the climate sensitivity parameter and produce probabilistic scenarios based on MAGICC and TCM precalculated runs. Extensions and future development of this model include the integration with IVA and integrated assessment models, such as simple agricultural emulators and climate-economy models (Estrada et al., 2020; Ignjacevic et al., 2020, 2021; Estrada and Botzen 2021); the inclusion of additional climate variables (e.g., minimum and maximum temperatures, sea level rise and bioclimatic indices), as well as complementary uni- and multivariate risk measures.

Declaration of competing interest

The authors declare that they have no known competing financial interests or personal relationships that could have appeared to influence the work reported in this paper.

Data availability

Data will be made available on request.

Acknowledgements

Francisco Estrada acknowledges financial support from DGAPA-UNAM through the projects PAPIIT IN110718 and IN111221 and from PINCC-UNAM.

Appendix A. Supplementary data

Supplementary data to this article can be found online at https://doi.org/10.1016/j.envsoft.2022.105528.

References

Adem, J., 1991. Review of the development and applications of the Adem thermodynamic climate model. Clim. Dynam. 5, 145–160. https://doi.org/10.1007/BF00251806.

Altamirano del Carmen, M.A., Estrada, F., Gay-Garciá, C., 2021. A new method for assessing the performance of general circulation models based on their ability to simulate the response to observed forcing. J. Clim. 34, 5385–5402. https://doi.org/10.1175/JCLI-D-20-0510.1.

Anthoff, D., Tol, R.S.J., 2014a. Climate policy under fat-tailed risk: an application of FUND. Ann. Oper. Res. 220, 223–237. https://doi.org/10.1007/s10479-013-1343-2.

Anthoff, D., Tol, R.S.J., 2014b. The Climate Framework for Uncertainty, Negotiation and Distribution (FUND), Technical Description, version 3.9.

Barrios, S., Bertinelli, L., Strobl, E., 2006. Climatic change and rural–urban migration: the case of sub-Saharan Africa. J. Urban Econ. 60, 357–371. https://doi.org/10.1016/J.JUE.2006.04.005.

Blanc, É., 2017. Statistical emulators of maize, rice, soybean and wheat yields from global gridded crop models. Agric. For. Meteorol. 236, 145–161. https://doi.org/10.1016/j.agrformet.2016.12.022.

Bony, S., Stevens, B., Held, I.H., et al., 2013. Carbon dioxide and climate: perspectives on a scientific assessment. In: Climate Science for Serving Society, pp. 391–413.

Cabré, M.F., Solman, S.A., Nuñez, M.N., 2010. Creating regional climate change scenarios over southern South America for the 2020's and 2050's using the pattern

scaling technique: validity and limitations. Clim. Change 98, 449–469. https://doi.org/10.1007/s10584-009-9737-5.
Callendar, G.S., 1938. The artificial production of carbon dioxide and its influence on temperature. Q. J. R. Meteorol. Soc. 64, 223–240. https://doi.org/10.1002/qj.49706427503.
Collins, M., Knutti, R., Arblaster, J., et al., 2013. Long-term climate change: projections, commitments and irreversibility. In: Climate Change 2013 the Physical Science Basis: Working Group I Contribution to the Fifth Assessment Report of the Intergovernmental Panel on Climate Change, pp. 1029–1136.
Conde, C., Estrada, F., Martínez, B., et al., 2011. Regional climate change scenarios for México. Atmósfera 24, 125–140.
Cox, P.M., Huntingford, C., Williamson, M.S., 2018. Emergent constraint on equilibrium climate sensitivity from global temperature variability. Nature 553, 319–322. https://doi.org/10.1038/nature25450.
Curry, J.A., Webster, P.J., 2011. Climate science and the uncertainty monster. Bull. Am. Meteorol. Soc. 92, 1667–1682.
De Dato, G., Pellizzaro, G., Cesaraccio, C., et al., 2008. Effects of Warmer and Drier Climate Conditions on Plant Composition and Biomass Production in a Mediterranean Shrubland Community. https://doi.org/10.3832/IFOR0418-0010039. http://iforest.sisef.org/1:39.
Deser, C., Phillips, A.S., Alexander, M.A., Smoliak, B.V., 2014. Projecting North American climate over the next 50 years: uncertainty due to internal variability. J. Clim. 27, 2271–2296. https://doi.org/10.1175/JCLI-D-13-00451.1.
Estrada, F., Botzen, W.J.W., 2021. Economic impacts and risks of climate change under failure and success of the Paris Agreement. Ann N Y Acad Sci nyas 14652. https://doi.org/10.1111/NYAS.14652.
Estrada, F., Botzen, W.J.W., Calderon-Bustamante, O., 2020. The Assessment of Impacts and Risks of Climate Change on Agriculture (AIRCCA) model: a tool for the rapid global risk assessment for crop yields at a spatially explicit scale. Spatial Econ. Anal. 15, 262–279. https://doi.org/10.1080/17421772.2020.1754448.
Fick, S.E., Hijmans, R.J., 2017. WorldClim 2: new 1-km spatial resolution climate surfaces for global land areas. Int. J. Climatol. 37, 4302–4315. https://doi.org/10.1002/joc.5086.
Forster, P., Ramaswamy, V., Artaxo, P., et al., 2007. Changes in atmospheric constituents and in radiative forcing. Chapter 2. In: Climate Change 2007. The Physical Science Basis. cambridge University press, Cambridge, p. 106.
Freeman, M.C., Wagner, G., Zeckhauser, R.J., 2015. Climate sensitivity uncertainty: when is good news bad? Philos. Trans. R. Soc. A Math. Phys. Eng. Sci. 373, 20150092 https://doi.org/10.1098/rsta.2015.0092.
Friedrich, T., Timmermann, A., Tigchelaar, M., et al., 2016. Nonlinear climate sensitivity and its implications for future greenhouse warming. Sci. Adv. 2, e1501923 https://doi.org/10.1126/sciadv.1501923.
Gay, C., Estrada, F., 2010. Objective probabilities about future climate are a matter of opinion. Clim. Change 99, 27–46. https://doi.org/10.1007/s10584-009-9681-4.
Hammitt, J.K., Lempert, R.J., Schlesinger, M.E., 1992. A sequential-decision strategy for abating climate change. Nat 357, 315–318. https://doi.org/10.1038/357315a0, 1992 3576376.
Herger, N., Sanderson, B.M., Knutti, R., 2015. Improved pattern scaling approaches for the use in climate impact studies. Geophys. Res. Lett. 42, 3486–3494. https://doi.org/10.1002/2015GL063569.
Hodler, R., Raschky, P.A., 2014. Economic shocks and civil conflict at the regional level. Econ. Lett. 124, 530–533. https://doi.org/10.1016/J.ECONLET.2014.07.027.
Hodrick, R.J., Prescott, E.C., 1997. Postwar U.S. Business cycles: an empirical investigation. J. Money Credit Bank. 29, 1. https://doi.org/10.2307/2953682.
Hsiang, S.M., Burke, M., Miguel, E., 2013. Quantifying the influence of climate on human conflict. Science 341, 1235367. https://doi.org/10.1126/science.1235367.
Ignjacevic, P., Botzen, W.J.W., Estrada, F., et al., 2020. CLIMRISK-RIVER: accounting for local river flood risk in estimating the economic cost of climate change. Environ. Model. Software 132. https://doi.org/10.1016/j.envsoft.2020.104784.
Ignjacevic, P., Estrada, F., Botzen, W.J.W., 2021. Time of emergence of economic impacts of climate change. Environ. Res. Lett. 16 https://doi.org/10.1088/1748-9326/AC0D7A, 074039.
IPCC, 2021. Climate Change 2021: the Physical Science Basis. IPCC.
IPCC, 2018. Impacts of 1.5°C of global warming on natural and human systems. In: Glob. Warm. 1.5°C. An IPCC Spec. Rep. Impacts Glob. Warm. 1.5°C above Pre-industrial Levels Relat. Glob. Greenh. Gas Emiss. Pathways, Context Strength. Glob. Response to Threat Clim. Chang.
IPCC-TGICA, 2007. General Guidelines on the Use of Scenario Data for Climate Impact and Adaptation Assessment.
Jaynes, E.T., 1957. Information theory and statistical mechanics. Phys. Rev. 106, 620–630. https://doi.org/10.1103/PhysRev.106.620.
Jaynes, E.T., Edwin, T., Bretthorst, G.L., 2003. Probability Theory : the Logic of Science. Cambridge University Press.
Jonko, A., Urban, N.M., Nadiga, B., 2018. Towards Bayesian hierarchical inference of equilibrium climate sensitivity from a combination of CMIP5 climate models and observational data. Clim. Change 149, 247–260. https://doi.org/10.1007/s10584-018-2232-0.
Knutti, R., 2010. The end of model democracy? Clim. Change 102, 395–404. https://doi.org/10.1007/s10584-010-9800-2.
Knutti, R., Rugenstein, M.A.A., 2015. Feedbacks, climate sensitivity and the limits of linear models. Philos. Trans. R. Soc. A Math. Phys. Eng. Sci. 373 https://doi.org/10.1098/RSTA.2015.0146.
Knutti, R., Sedláček, J., 2012. Robustness and uncertainties in the new CMIP5 climate model projections. Nat. Clim. Change 3, 1–5. https://doi.org/10.1038/nclimate1716.
Knutti, R., Furrer, R., Tebaldi, C., et al., 2010. Challenges in combining projections from multiple climate models. J. Clim. 23, 2739–2758. https://doi.org/10.1175/2009JCLI3361.1.
Knutti, R., Rugenstein, M.A.A., Hegerl, G.C., 2017. Beyond equilibrium climate sensitivity. Nat. Geosci. 10, 727–736.
Kravitz, B., Lynch, C., Hartin, C., Bond-Lamberty, B., 2017a. Exploring precipitation pattern scaling methodologies and robustness among CMIP5 models. Geosci. Model Dev. (GMD) 10, 1889–1902. https://doi.org/10.5194/gmd-10-1889-2017.
Kravitz, B., Lynch, C., Hartin, C., Bond-Lamberty, B., 2017b. Exploring precipitation pattern scaling methodologies and robustness among CMIP5 models. Geosci. Model Dev. (GMD) 10, 1889–1902. https://doi.org/10.5194/gmd-10-1889-2017.
Lewis, N., Curry, J.A., 2015. The implications for climate sensitivity of AR5 forcing and heat uptake estimates. Clim. Dynam. 45, 1009–1023. https://doi.org/10.1007/s00382-014-2342-y.
Lynch, C., Hartin, C., Bond-Lamberty, B., Kravitz, B., 2017. An open-access CMIP5 pattern library for temperature and precipitation: description and methodology. Earth Syst. Sci. Data 9, 281–292. https://doi.org/10.5194/essd-9-281-2017.
Maier-Reimer, E., Hasselmann, K., 1987. Transport and storage of CO2 in the ocean – an inorganic ocean-circulation carbon cycle model. Clim. Dynam. 2, 63–90. https://doi.org/10.1007/BF01054491.
Meinshausen, M., Raper, S.C.B., Wigley, T.M.L., 2011a. Emulating coupled atmosphere-ocean and carbon cycle models with a simpler model, MAGICC6 - Part 1: model description and calibration. Atmos. Chem. Phys. 11, 1417–1456. https://doi.org/10.5194/acp-11-1417-2011.
Meinshausen, M., Smith, S.J., Calvin, K., et al., 2011b. The RCP greenhouse gas concentrations and their extensions from 1765 to 2300. Clim. Change 109, 213–241. https://doi.org/10.1007/s10584-011-0156-z.
Meinshausen, M., Wigley, T.M.L., Raper, S.C.B., 2011c. Emulating atmosphere-ocean and carbon cycle models with a simpler model, MAGICC6 - Part 2: Applications. Atmos. Chem. Phys. https://doi.org/10.5194/acp-11-1457-2011.
Mendlik, T., Gobiet, A., 2016. Selecting climate simulations for impact studies based on multivariate patterns of climate change. Clim. Change 135, 381–393. https://doi.org/10.1007/s10584-015-1582-0.
Mitchell, T.D., 2003. Pattern scaling: an examination of the accuracy of the technique for describing future climates. Clim. Change 60, 217–242. https://doi.org/10.1023/A:1026035305597.
Moore, F.C., Rising, J., Lollo, N., et al., 2018. Mimi-PAGE, an open-source implementation of the PAGE09 integrated assessment model. Sci. Data 5, 180187. https://doi.org/10.1038/sdata.2018.187.
Nicholls, Z., Meinshausen, M., Lewis, J., et al., 2021. Reduced complexity model Intercomparison project phase 2: synthesizing Earth system knowledge for probabilistic climate projections. Earth's Future 9, e2020EF001900. https://doi.org/10.1029/2020EF001900.
Nordhaus, W.D., Boyer, J., 2003. Warming the World: Economic Models of Global Warming. MIT press.
Notz, D., 2015. How well must climate models agree with observations? Philos. Trans. R. Soc. A Math. Phys. Eng. Sci. 373, 20140164 https://doi.org/10.1098/rsta.2014.0164.
Osborn, T.J., Wallace, C.J., Lowea, J.A., Bernie, D., 2018. Performance of pattern-scaled climate projections under high-end warming. Part I: surface air temperature over land. J. Clim. 31, 5667–5680. https://doi.org/10.1175/JCLI-D-17-0780.1.
Pithan, F., Mauritsen, T., 2014. Arctic amplification dominated by temperature feedbacks in contemporary climate models. Nat. Geosci. 7, 181–184. https://doi.org/10.1038/ngeo2071.
Potter, T.D., Colman, B.R., 2003. Handbook of Weather, Climate, and Water : Atmospheric Chemistry, Hydrology, and Societal Impacts. Wiley-Interscience.
Puente, G.B., Perez, F., Gitter, R.J., 2016. The effect of rainfall on migration from Mexico to the United States. Int. Migr. Rev. 50, 890–909. https://doi.org/10.1111/imre.12116.
Ramaswamy, V., Boucher, O., Haigh, J., et al., 2001. Radiative forcing of climate change. In: Climate Change 2001: the Scientific Basis, Contribution of Working Group I to the Third Assessment Report of the Intergovernmental Panel on Climate Change.
Rogelj, J., Meinshausen, M., Sedláček, J., Knutti, R., 2014. Implications of potentially lower climate sensitivity on climate projections and policy. Environ. Res. Lett. 9, 031003 https://doi.org/10.1088/1748-9326/9/3/031003.
Sanderson, B.M., Knutti, R., Caldwell, P., 2015. A representative democracy to reduce interdependency in a multimodel ensemble. J. Clim. 28, 5171–5194. https://doi.org/10.1175/JCLI-D-14-00362.1.
Santer, B.D., Wigley, T.M.L., Schlesinger, M.E., Mitchell, J.F.B., 1990. Developing climate scenarios from equilibrium GCM results. Report/Max-Planck-Institut. für Meteorol. 47.
Santer, B.D., Bonfils, C.J.W., Fu, Q., et al., 2019. Celebrating the anniversary of three key events in climate change science. Nat. Clim. Change 9, 180–182.
Schneider, S.H., Thompson, S.L., 1981. Atm)ospheric CO 2 and climate: importance of the transient response. J. Geophys. Res. 86, 3135. https://doi.org/10.1029/JC086iC04p03135.
Stephenson, D.B., Collins, M., Rougier, J.C., Chandler, R.E., 2012. Statistical problems in the probabilistic prediction of climate change. Environmetrics 23, 364–372. https://doi.org/10.1002/env.2153.
Stevens-Rumann, C.S., Kemp, K.B., Higuera, P.E., et al., 2018. Evidence for declining forest resilience to wildfires under climate change. Ecol. Lett.
Stocker, T.F., Qin, D., Plattner, G.K., et al., 2013. Climate Change 2013 the Physical Science Basis: Working Group I Contribution to the Fifth Assessment Report of the Intergovernmental Panel on Climate Change.

Tan, I., Storelvmo, T., Zelinka, M.D., 2016. Observational constraints on mixed-phase clouds imply higher climate sensitivity. Science 352 (80), 224–227. https://doi.org/10.1126/science.aad5300.

Taylor, K.E., Stouffer, R.J., Meehl, G.A., 2012. An overview of CMIP5 and the experiment design. Bull. Am. Meteorol. Soc. 93, 485–498.

Tebaldi, C., Arblaster, J.M., 2014. Pattern scaling: its strengths and limitations, and an update on the latest model simulations. Clim. Change 122, 459–471. https://doi.org/10.1007/s10584-013-1032-9.

Tebaldi, C., Knutti, R., 2018. Evaluating the accuracy of climate change pattern emulation for low warming targets. Environ. Res. Lett. 13, 055006 https://doi.org/10.1088/1748-9326/aabef2.

Tol, R.S.J., 2019a. Climate Economics: Economic Analysis of Climate, Climate Change and Climate Policy, Second. Edward Elgar Publishing.

Tol, R.S.J., 2019b. Matlab Scripts for FUND 4.0 MN.

Tol, R.S.J., Fankhauser, S., 1998. On the representation of impact in integrated assessment models of climate change. Environ. Model. Assess. 3, 63–74. https://doi.org/10.1023/A:1019050503531.

Weigel, A.P., Knutti, R., Liniger, M.A., Appenzeller, C., 2010. Risks of model weighting in multimodel climate projections. J. Clim. 23, 4175–4191. https://doi.org/10.1175/2010JCLI3594.1.

Wigley, T.M.L., 1995. MAGICC and SCENGEN: integrated models for estimating regional climate change in response to anthropogenic emissions. Stud. Environ. Sci. 65, 93–94. https://doi.org/10.1016/S0166-1116(06)80197-4.

World Bank, 2016. High and Dry: Climate Change, Water, and the Economy. World Bank.

Xu, Y., Gao, X., Giorgi, F., 2010. Upgrades to the reliability ensemble averaging method for producing probabilistic climate-change projections. Clim. Res. 41, 61–81. https://doi.org/10.3354/cr00835.

Zelazowski, P., Huntingford, C., Mercado, L.M., Schaller, N., 2018. Climate pattern-scaling set for an ensemble of 22 GCMs – adding uncertainty to the IMOGEN version 2.0 impact system. Geosci. Model Dev. (GMD) 11, 541–560. https://doi.org/10.5194/gmd-11-541-2018.